Controllable enzymatic superactivity of α-chymotrypsin activated by the electrostatic interaction with cationic gemini surfactants

Zheng Yue ,[a‡] Meihuan Yao, [a‡] Guangyue Bai,*[a] Jiuxia Wang,[a,b] Kelei Zhuo,[a] Jianji Wang[a] and Yujie Wang*[b]

[a]*Collaborative Innovation Center of Henan Province for Green Manufacturing of Fine Chemicals, Key Laboratory of Green Chemical Media and Reactions, Ministry of Education, School of Chemistry and Chemical Engineering, Henan Normal University, Xinxiang, Henan 453007, P. R. China.* [b] *School of Chemistry and Chemical Engineering, Henan Institute of Science and Technology, Xinxiang, Henan 453003, P. R. China.*

* Corresponding authors. baiguangyue@htu.cn (G. Bai); yujiewang2001@163.com (Y. Wang).

Electronic Supplementary Information

I. The change of 2-N concentration in the process of the enzymatic reaction

The initial rate was obtained by the initial slope of the curve of concentration of 2-N produced under catalysis of α-CT as a function of time, and three typical curves were presented in **Fig. S1**. The concentration of 2-N was measured by the absorbance at wavelength of 328 nm. The results show that the curves have a linear function before about 120 seconds and the regression coefficient is about 0.999.

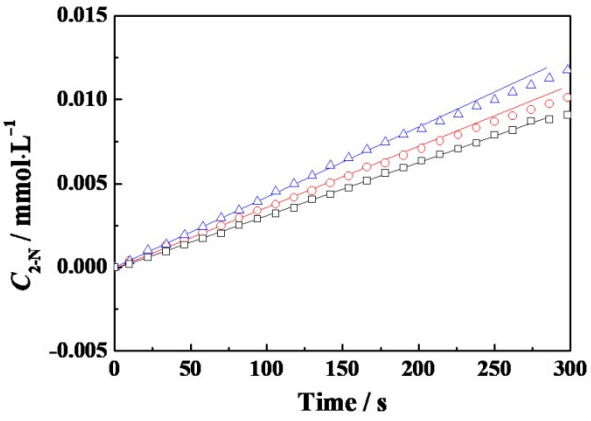

Fig. S1 Time course of 2-N formation from the hydrolysis of 2-NA catalyzed by α-CT in the buffered $C_{12}C_{10}C_{12}Br_2$ at 298.15 K. Conditions: $C_{2\text{-NA}}$ = 0.081 mmol·L^{-1}; $C_{\alpha\text{-CT}}$ = 0.1 g·L^{-1} and the concentrations (mmol·L^{-1}) of $C_{12}C_{10}C_{12}Br_2$ were (●) 0.005, (ᔓ) 0.010 and (□) 0.040, respectively. The original data (Abs) were recorded automatically by one data per 2 second and for clear view less data were shown in the curves.

II. UV-vis spectra of 2-NA and 2-N

Both 2-NA and 2-N have larger solubilities in the presence of surfactant micelles. Their

absorbance spectra can prove the solubilization and assess their location in the micellar psuedophase. **Fig. S2** shows the UV-vis spectra of 2-NA, where two peaks at 273 nm and 316 nm were chosen to distinguish the wavelength shifts. **Fig. S3** gives the results in the UV-vis spectra of 2-N in surfactant solutions, and the absorbance peaks at about 328 nm were marked to distinguish the wavelength shifts with the surfactant concentrations.

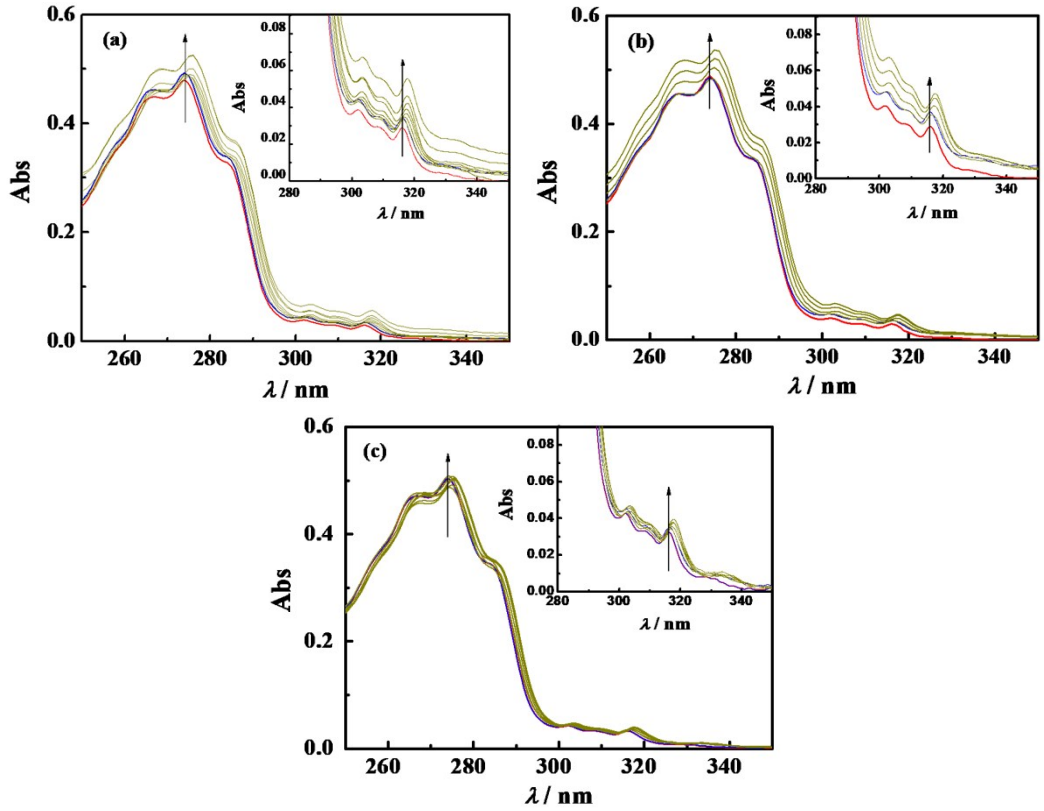

Fig. S2 UV-vis spectra of 0.1 mmol·L^{-1} 2-NA in various concentrations of buffered surfactant at 25 °C. (**a**) $C_{12}C_2C_{12}Br_2$ concentrations (mmol·L^{-1}): 0, 0.13, 0.50, 1.40, 3.00, 4.00, 6.00, 8.00, 10.0; (**b**) $C_{12}C_6C_{12}Br_2$ concentrations (mmol·L^{-1}): 0, 0.17, 0.70, 1.70, 3.00, 5.00; (**c**) $C_{12}C_{10}C_{12}Br_2$ concentrations (mmol·L^{-1}): 0, 0.06, 0.26, 0.50, 1.00, 2.00, 3.00, 4.00, 5.00. The arrows point to the direction of increasing surfactant concentration for the respective spectrum.

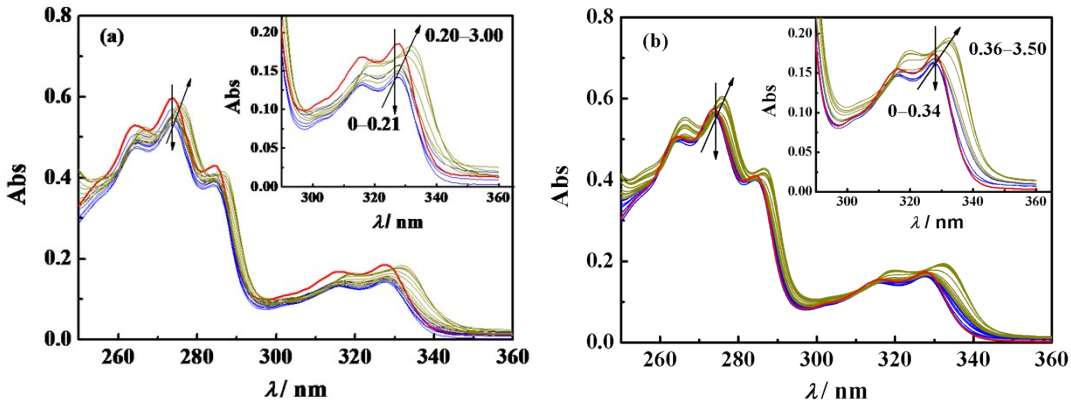

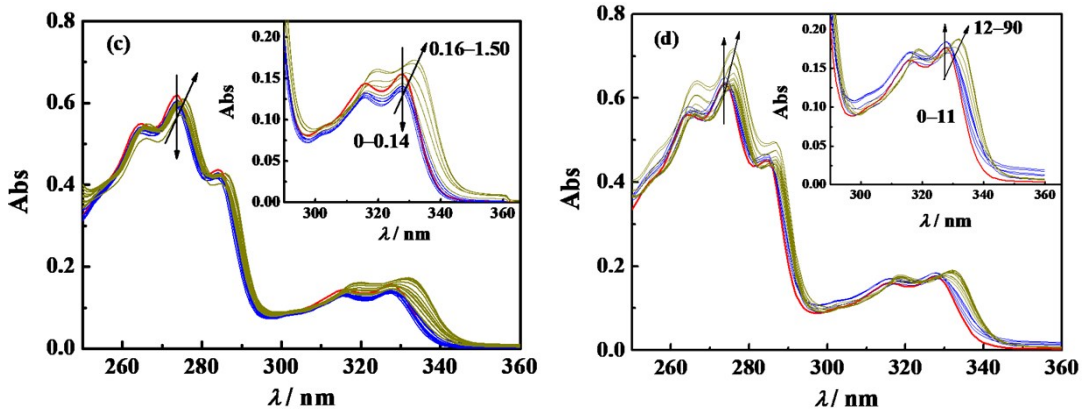

Fig. S3 UV-vis spectra of 0.14 mmol·L^{-1} 2-N in various concentrations of buffered surfactant at 25 °C. (**a**) 12-2-12 concentrations (mmol·L^{-1}): 0, 0.03, 0.09, 0.15, 0.20, 0.25, 0.30, 0.50, 1.00, 2.00, 3.00; (**b**) 12-6-12 concentrations (mmol·L^{-1}): 0, 0.05, 0.10, 0.20, 0.30, 0.36, 0.40, 0.80, 1.50, 2.50, 3.50; (**c**) 12-10-12 concentrations (mmol·L^{-1}): 0, 0.02, 0.04, 0.06, 0.10, 0.14, 0.16, 0.25, 0.50; 1.00, 1.50; (**d**) DTAB concentrations (mmol·L^{-1}): 0, 3.0, 6.0, 8.0, 10.0, 11.0, 12.0, 14.0, 20.0, 50.0, 90.0. The arrows point to the direction of increasing surfactant concentration for the respective spectrum.

III. Conductivity measurements for titrating the buffered surfactant into buffer solution (PBS, pH7.3)

The conductivity of surfactant solution was measured with a DDJS-308A conductimeter (DJS-1C electrode, China) in a double-walled vessel thermostatted by flowing water at T = 298.15 K. The conductimeter was calibrated with a standard KCl solution (0.1 mol·dm^{-3}) of known conductivity.

The concentrated $C_{12}C_SC_{12}Br_2$ (S = 2, 6, 10) or DTAB solutions (PBS, pH7.3) were titrated into PBS with the same concentration and pH value. **Fig. S4** shows variation of the differences between the conductivities at the successive additions of the buffered surfactant and at the initial PBS as a function of surfactant concentration, reflecting the effect of the interaction of the surfactant with negative phosphate ion. The conductivity decreases as the surfactant concentration increases in a dilute concentration range due to the simultaneous decrease of the conductive contributions of HPO_4^{2-} and the surfactant cation against the increase of counterionic Br^- contribution. Though the sensitivity of conductivity measurement is reduced at higher PBS concentration, it is out of question that the conductivity differences rise up as the PBS concentration increases.

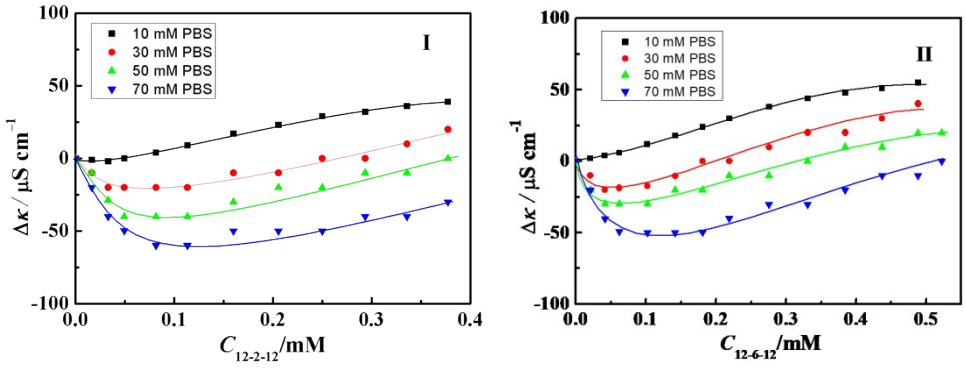

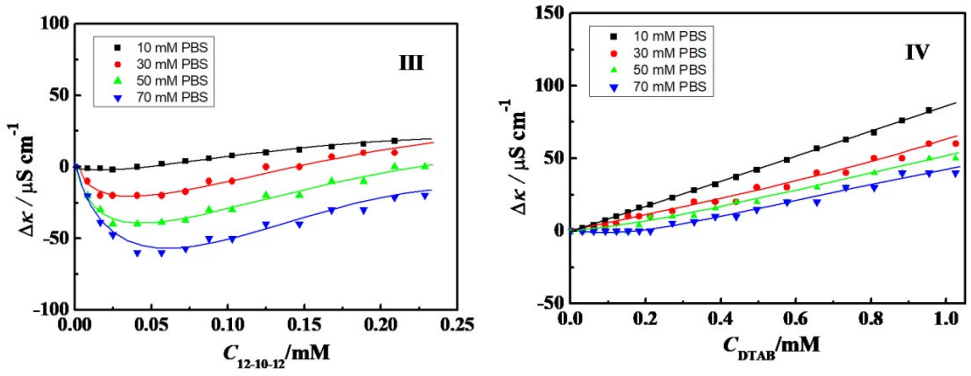

Fig. S4 Variation of the conductivity difference ($\Delta\kappa$) as a function of the concentration of $C_{12}C_2C_{12}Br_2$ (**I**), $C_{12}C_6C_{12}Br_2$ (**II**), $C_{12}C_{10}C_{12}Br_2$ (**III**) and DTAB (**IV**) in PBS (pH7.3) of 10, 30, 50, and 70 mmol·L^{-1} at 298.15 K.

IV. ITC results for titration of the buffered $C_{12}C_SC_{12}Br_2$ (S = 2, 6, 10) solution into 10 mmol·L^{-1} PBS (pH7.3)

When a concentrated surfactant solution is titrated into buffer solution, the micellization process occurs, which can be detected by following the change of observed enthalpy (ΔH_{obs}) with concentration of surfactant (C_i). From the two breaks of calorimetric curve (ΔH_{obs} vs. C_i), the enthalpy change of micellization and cmc can be obtained as shown in **Fig. S5.**

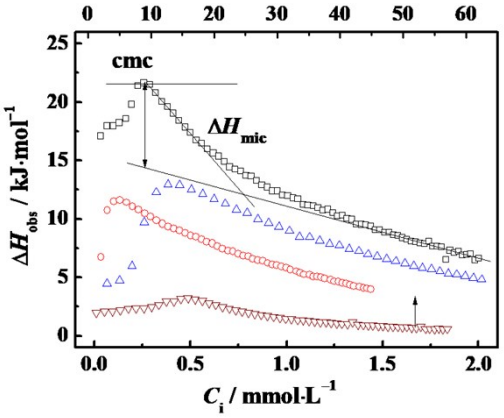

Fig. S5 Variation of observed enthalpy (ΔH_{obs}) with surfactant concentration (C_i) for titrating a concentrated $C_{12}C_SC_{12}Br_2$ (S = 2, 6, 10) or DTAB solution into PBS of 10 mmol·L^{-1} (pH7.3) at 298.15 K. The symbols mark different surfactants as follows: (□) $C_{12}C_2C_{12}Br_2$; (Δ) $C_{12}C_6C_{12}Br_2$; (○) $C_{12}C_{10}C_{12}Br_2$; (∇) DTAB. The upper abscissa represents only DTAB concentrations.

V. ITC results for titrating the concentrated $C_{12}C_SC_{12}Br_2$ (S = 2, 6, 10) and DTAB solutions into different concentration *α*-CT solutions

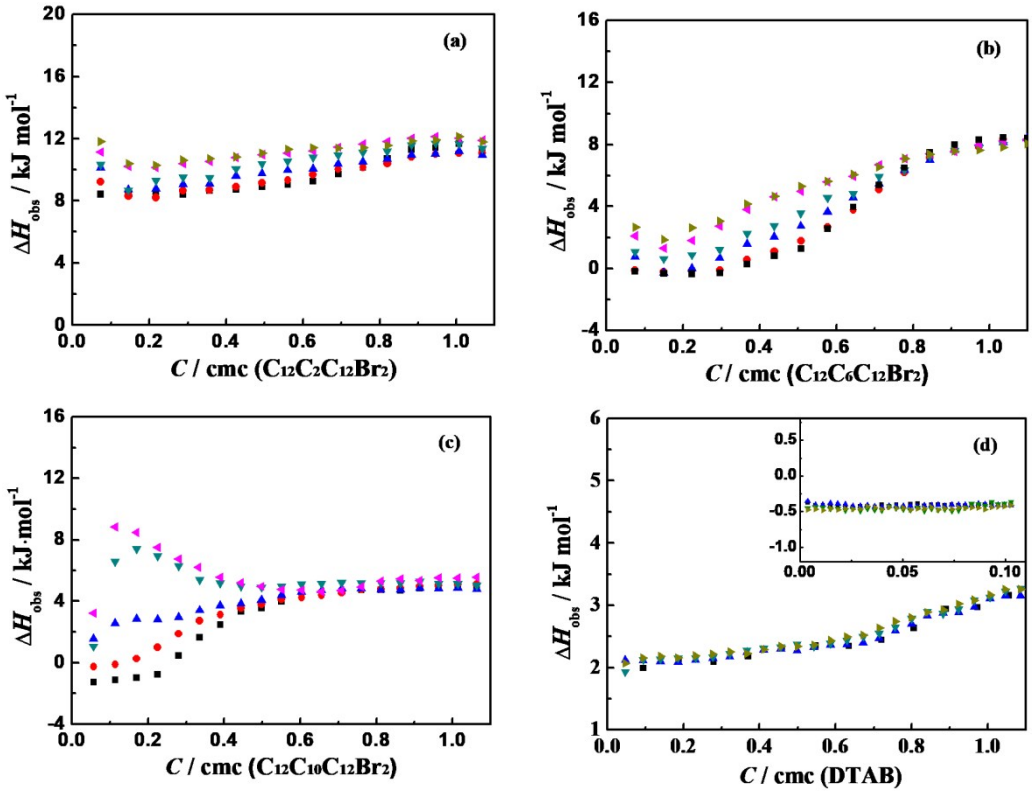

Fig. S6 Variation of the observed enthalpy with surfactant concentration ratio C/cmc for the titration of $C_{12}C_SC_{12}Br_2$ (S = 2 (**a**), S = 6 (**b**), S = 10 (**c**)) or DTAB (**d**) into α-CT aqueous solution (10 mmol·L^{-1} PBS, pH7.3) at 298.15 K**.** The symbols mark the α-CT concentration (g·L^{-1}) of: (○) 0; (↯) 0.05; (▲) 0.10; (❑) 0.20; (♦) 0.30 and (◆) 0.40, respectively. The surfactant concentration in the syringe is 3.0 mmol·L^{-1} for $C_{12}C_2C_{12}Br_2$, 4.0 mmol·L^{-1} for $C_{12}C_6C_{12}Br_2$, 2.0 mmol·L^{-1} for $C_{12}C_{10}C_{12}Br_2$ and 200 mmol·L^{-1} for DTAB. The inset plot in frame (d) shows an enlargement in the dilute concentration range of the ratio C/cmc < 0.1 that was titrated by dilute DTAB solution of 16 mmol·L^{-1}. The data in frame (c) come from the same experiment as given in reference [26] but the abscissa was changed from $C_{12\text{-}10\text{-}12}$ to C/cmc ($C_{12}C_{10}C_{12}Br_2$).

VI. ITC results for titrating the concentrated $C_{12}C_6C_{12}Br_2$ solution into different concentration PBS and corresponding buffered α-CT solution

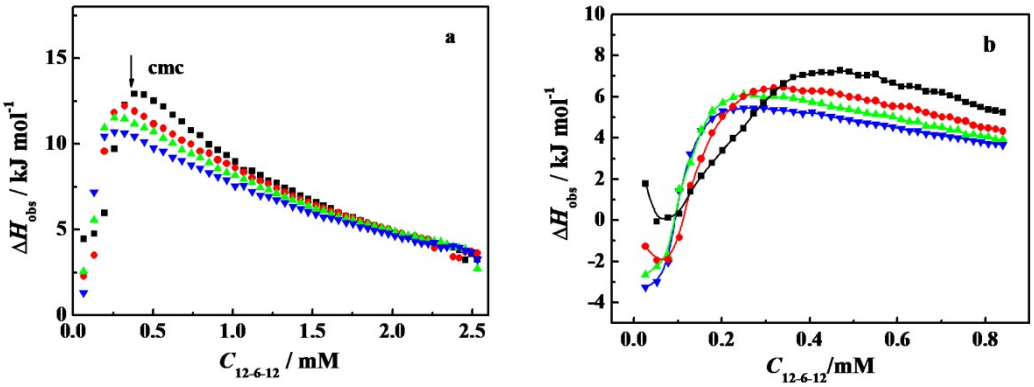

Fig. S7 Variation of the observed enthalpy (ΔH_{obs}) with surfactant concentration at 298.15 K. (**a**) in pure PBS and (b) in buffered α-CT (0.30 g·L^{-1}). The PBS (pH7.3) concentrations are (■) 10, (●) 30, (❒) 50, and (❑) 70 mmol·L^{-1}, respectively.

VII. Fluorescence measurements of 0.10 g·L^{-1} α-CT after incubation of 120 min in the buffered $C_{12}C_SC_{12}Br_2$ and DTAB solutions

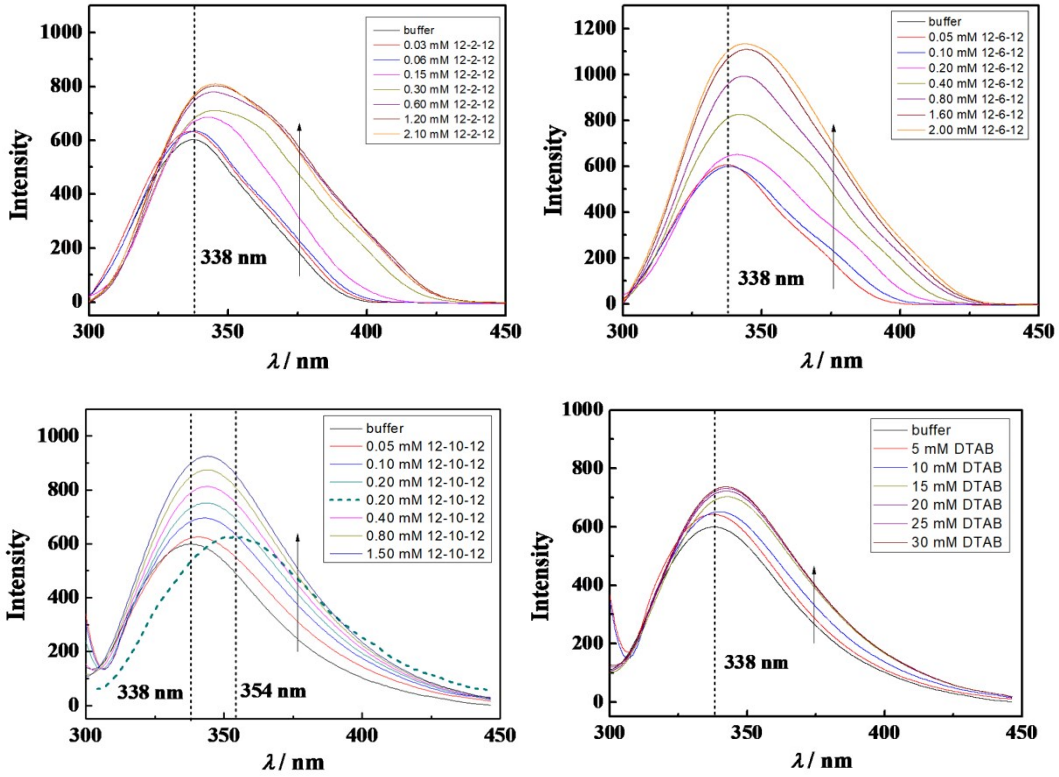

Fig. S8 The fluorescence spectra of 0.10 g·L^{-1} α-CT after incubated for120 min and for 4 days (short dash in the frame with $C_{12}C_{10}C_{12}Br_2$) at 298K in $C_{12}C_SC_{12}Br_2$ (S = 2, 6, 10) and DTAB solutions. The arrows indicate the direction of the concentration increase. The other information was shown in the legend frames.

VIII. DSC measurements of the thermal stability of α-CT

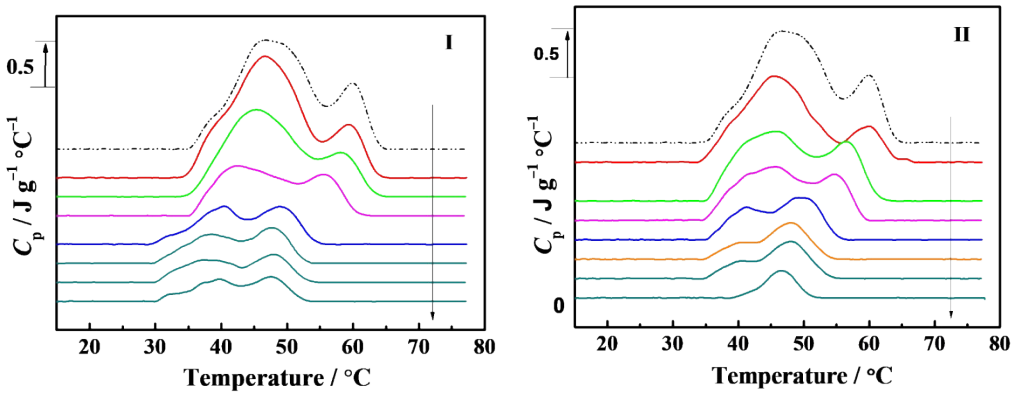

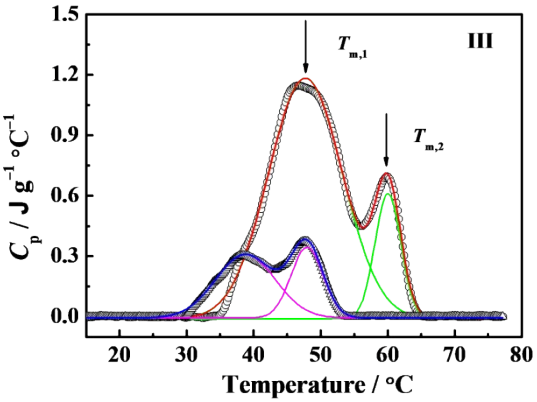

Fig. S9 DSC thermograms for 0.5 g·L^{-1} α-CT solutions incubated 20 min in buffer and buffered $C_{12}C_2C_{12}Br_2$ (**I**) with concentrations (mmol·L^{-1}) of 0; 0.02; 0.04; 0.08; 0.25; 0.30; 0.35; 0.40, respectively, and $C_{12}C_6C_{12}Br_2$ (**II**) with concentrations (mmol·L^{-1}) of 0; 0.02; 0.05; 0.08; 0.16; 0.3; 0.4; 0.5, respectively. The arrows on the vertical axis of frame (**I**) or (**II**) point to the endothermic direction. The figure (**III**) gives an example for multi-peak fitting curves in pure PBS (○) and $C_{12}C_2C_{12}Br_2$ of 0.3 mmol·L^{-1} (Δ), respectively, with Gaossian function.

Table S1 Thermodynamic parameters $T_{m,1}$, $T_{m,2}$, ΔH_1 and ΔH_2 for α-CT in PBS with different $C_{12}C_2C_{12}Br_2$ concentrations

$C_{12}C_2C_{12}Br_2$ (mmol·L^{-1})	$T_{m,1}$ (°C)	ΔH_1 (J·g^{-1})	$T_{m,2}$ (°C)	ΔH_2 (J·g^{-1})
0	48.7±0.5	16.5±0.2	60.0±0.3	3.0±0.3
0.02	47.5±0.5	17.4±0.2	59.5±0.3	2.6±0.3
0.04	46.7±0.5	12.0±0.2	58.1±0.3	3.1±0.3
0.08	44.4±0.5	9.6±0.2	55.7±0.3	2.4±0.3
0.10	42.7±0.5	8.2±0.2	53.3±0.3	2.2±0.3
0.12	41.5±0.5	6.7±0.2	51.1±0.3	2.7±0.3
0.25	40.9±0.5	4.1±0.2	49.3±0.3	2.4±0.3
0.3	39.8±0.5	3.5±0.2	48.0±0.3	2.1±0.3
0.35	39.2±0.5	2.6±0.2	48.0±0.3	1.7±0.3
0.40	40.4±0.5	2.7±0.2	48.0±0.3	1.3±0.3

Table S2 Thermodynamic parameters $T_{m,1}$, $T_{m,2}$, ΔH_1 and ΔH_2 for α-CT in PBS with different $C_{12}C_6C_{12}Br_2$ concentrations

$C_{12}C_6C_{12}Br_2$ (mmol·L^{-1})	$T_{m,1}$ (°C)	ΔH_1 (J·g^{-1})	$T_{m,2}$ (°C)	ΔH_2 (J·g^{-1})
0	47.7±0.5	16.5±0.2	60.0±0.3	3.0±0.3
0.02	45.7±0.5	11.4±0.2	59.7±0.3	2.1±0.3
0.05	45.0±0.5	9.8±0.2	56.4±0.3	3.6±0.3
0.08	44.8±0.5	7.4±0.2	54.9±0.3	2.2±0.3
0.10	43.3±0.5	6.0±0.2	52.5±0.3	2.4±0.3
0.16	41.5±0.5	2.7±0.2	49.8±0.3	3.1±0.3
0.30	40.3±0.5	1.2±0.2	48.0±0.3	2.7±0.3
0.40	40.1±0.5	1.1±0.2	47.8±0.3	2.8±0.3
0.50	40.0±0.5	0.5±0.1	46.5±0.3	1.7±0.3

IX. Zeta-potential measurements of α-CT in PBS

The zeta-potential was determined by Nano ZS-90 (Malvern, U.K.). Light of λ = 633 nm from a solid-state He-Ne laser (4.0 mW) was used as the incident beam. All sample solutions were filtered through a 0.22 μm hydrophilic PVDF membrane filter. The measurements were performed at 298.2 ± 0.2 K and at 90° scattering angle. The results are shown in Table S3. The data were measured at least ten times and given as an average value along with the corresponding standard deviation(SD).

Table S3 Zeta-potetial of α-CT in PBS with different concentrations at 298.2 K

PBS / mM	10	15	20	25	30	50
Mean / mV	-5.8	-7.9	-10.2	-8.2	-6.9	-7.8
SD	1.5	2.3	4.3	2.9	1.8	2.2

X. The molecular structure of the studied gemini surfactants

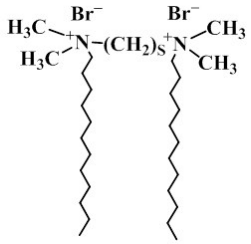

Scheme S1 The molecular structure of gemini surfactants $C_{12}C_SC_{12}Br_2$ (S = 2, 6, 10).